Effects of imaginary and real rotations on QCD matters

Gaoqing Cao
School of Physics and Astronomy, Sun Yat-sen University, Zhuhai 519088, China

(Received 10 October 2023; accepted 20 November 2023; published 2 January 2024)

Inspired from perturbative calculations, this work introduces imaginary ($\Omega_{\rm I}$) and real (Ω) rotation effects to the pure $SU(3)$ gauge potentials simply through variable transformations: the empirical Polyakov loop (PL) potentials can be rewritten as functions of the imaginary chemical potentials of gluons and ghosts ($q_{\rm ij}$), and the transformations are taken as $q_{\rm ij} \to q_{\rm ij} \pm \Omega_{\rm I}/T$ and $q_{\rm ij} \to q_{\rm ij} \pm i\Omega/T$, respectively. For the PL potential of Fukushima (V_1), a smaller imaginary rotation $\Omega_{\rm I}$ tends to suppress PL at all temperatures, and the deconfinement transition keeps of the first order. However, for the PL potential of the Munich group (V_2), $\Omega_{\rm I}$ tends to enhance PL at low temperature T, consistent with lattice simulations, but suppresses PL at high T, consistent with perturbative calculations. Moreover, the deconfinement alters from first order to crossover with increasing $\Omega_{\rm I}$ as is expected from lattice simulations. On the other hand, the real rotation Ω tends to enhance PL at relatively low T for both potentials, and the (pseudo)critical temperature decreases with Ω as expected. Therefore, we find that analytic continuation of the phase diagram from imaginary to real rotation is not necessarily valid in the nonperturbative region. Finally, we apply the more successful PL potential V_2 to the Polyakov–Nambu–Jona-Lasinio model and discover that $\Omega_{\rm I}$ tends to break chiral symmetry while Ω tends to restore it. Especially, the modified model is even able to qualitatively explain the lattice result that a larger T would catalyze chiral symmetry breaking for a large $\Omega_{\rm I}$.

DOI: 10.1103/PhysRevD.109.014001

I. INTRODUCTION

Recently, rotational or vortical effects have been of great interests to both theorists and experimentalists in high-energy nuclear physics [1]. Mainly, three aspects of rotation are extensively concerned in the literature: the anomalous transport phenomena, the phase diagrams of QCD, and the polarizations of hyperons and ϕ mesons. The former two are more of theoretical interests and have been explored with a variety of methods or effective models, while the last closely connects theories to experiments and promotes mutual developments. The earliest study of vortex involved anomalous transport is the chiral vortical effect [2,3], which was proposed right after the chiral magnetic effect [4,5] inspired from the similar polarization effects of rotation and magnetic field. Later, more anomalous phenomena were discovered, such as the chiral vortical separation effect [6], magnetovorticity effect [7], and chiral electric vortical effect [8,9]. In 2005, Liang and Wang proposed searching for the global polarization of hyperons in heavy ion collisions [10], but no significant signal was detected in the high-energy peripheral heavy ion collisions. The interests were renewed in 2016 when significant signals were found at smaller values of collision energy [11], and the local polarizations were explored for the first time in both the longitudinal and transversal directions [12–20].

If one translates the polarization signals into the angular velocities of rotation, the magnitude was evaluated to be as large as $\Omega = 9 \times 10^{21}$ s^{-1} [11]; thus, the quark-gluon plasma was regarded as the most vortical fluid in the Universe. In natural units, the rotation velocity is $\Omega = 6$ MeV, and the effective chemical potential $l\Omega$ is comparable to the QCD scale $\Lambda_{\rm QCD} \sim 200$ MeV for the angular momentum $l \geq 30$. Since then, the effects of rotation on QCD phases were extensively studied including the traditional topics such as chiral symmetry and confinement [21–23] and the possibilities of color superconductivity [21], pion superfluidity [24–26], and rho meson superconductivity [27,28]. The first studies of such rotational effects were carried out in the chiral effective Nambu–Jona-Lasinio (NJL) model where quarks are the elementary degrees of freedom [21–23]. It was found that rotation tends to suppress pairing states with zero angular momentum, such as chiral condensates and two-flavor color superconductive (2SC) diquark condensates [21]. Later, the Klein-Gordon theory predicted that pion superfluidity could appear in a QCD system with parallel magnetic field and rotation [24], which was then confirmed by the studies in the NJL model [25,26]. Furthermore, such a circumstance was carefully checked in advance, and rho meson superconductivity was found to be more favored for a larger magnetic field [28].

These years, several lattice QCD (LQCD) simulations were carried out to understand the features of confinement and chiral symmetry in the presence of an imaginary rotation $\Omega_{\rm I}$ as there is no sign problem [29–31]. There seem contradictions among the results. For homogeneous

phases, $\Omega_{\rm I}$ would break confinement and restore chiral symmetry, and hence the pseudocritical temperature $T_{\rm c}$ would decrease with $\Omega_{\rm I}$ for a finite system [29,31]. For inhomogeneous phases, $\Omega_{\rm I}$ would suppress deconfinement, and $T_{\rm c}$ would increase with $\Omega_{\rm I}$ [30]. In the case of a real rotation, there is sign problem in principle as the effective chemical potentials $l\Omega$ would render the action complex valued [22]. So, one usually supposes the analytic continuation to be valid for finite rotations and obtains the phase diagram of Ω from that of $\Omega_{\rm I}$. Then, if one translates the homogeneous results, the conclusion would be that $T_{\rm c}$ increases with Ω [29,31], opposite to the findings in the NJL model [21–23]. To understand that, perturbative calculations and effective models had been applied to such systems, but most of the results turned out to be "unsuccessful" [32–35] except a few studies [36,37]. Especially, the perturbative calculations started with the completely deconfined phase at high temperature, where the PL is 1 and only gluons are the relevant degrees of freedom, and found that $\Omega_{\rm I}$ would reinforce confinement [32]. However, ghosts are the reasons of confinement at low temperature in the language of LQCD [38] and would also be directly affected by rotations [32]. In that sense, the perturbative results do not necessarily contradict with the LQCD simulations, where the PL was found to be much less than 1 around $T_{\rm c}$ [38].

In this work, we want to find a way to reasonably introduce rotation effects into the gluon sector of QCD and then check whether it is reliable or not to obtain the real rotation effect simply through analytic continuation of the LQCD data. The paper is organized as follows. In Sec. II, we try to introduce the effects of imaginary and real rotations into the pure $SU(3)$ gauge theory in Sec. II A and compare the results of two empirical Polyakov loop (PL) potentials in Secs. II B 1 and II B 2, respectively. Then, we extend the work to the three-flavor PNJL model to study the properties of QCD system more realistically in Sec. III. Finally, a summary will be given in Sec. IV.

II. PURE $SU(3)$ GAUGE THEORY

A. Introduction of rotation effects

In the pure $SU(3)$ gauge theory, the Polyakov loop serves as a true order parameter for the Z_3 center symmetry of the gauge group, which is directly related to confinement [38]. It is defined as $L \equiv \frac{1}{N_{\rm c}}{\rm tr}_{\rm c} e^{ig\int_0^\beta \mathcal{A}_4 {\rm d}\tau}$, where $\beta = 1/T$ is inverse temperature and $\mathcal{A}_4 \equiv A_4^a \frac{\lambda_{\rm c}^a}{2}$ is the temporal component of the non-Abelian gauge field with $\lambda_{\rm c}^a (a = 1\text{–}8)$ the Gell-Mann matrices in color space. Usually, the expectation value of $\mathcal{A}_4$ is taken as a diagonal and traceless constant matrix, that is, $g\mathcal{A}_4 = T{\rm diag}(q_1, q_2, q_3)$ with $q_1 + q_2 + q_3 = 0$ [38]; then, it follows that

$$L(q_1, q_2, q_3) = \frac{1}{N_{\rm c}}(e^{iq_1} + e^{iq_2} + e^{iq_3}). \tag{1}$$

With respect to that, imaginary color chemical potentials are introduced to both gluons and ghosts, that is,

$$\pm q_{31}, \qquad \pm q_{21}, \qquad \pm q_{32} \tag{2}$$

with $q_{\rm ij} = q_i - q_j$ [38]. Since $\pm q_{\rm ij}$ always show up together, we only take $q_{\rm ij}(i > j)$ as the independent variables in the following.

According to the perturbative study in Ref. [32], the imaginary rotation $\Omega_{\rm I}$ introduces extra imaginary chemical potentials to both gluons and ghosts. And in the deconfined phase, the effect can be equivalently accounted for by simply taking two branches of variable transformations to $q_{\rm ij}$ in the thermodynamic potential of physical gluons, that is,

$$q_{\rm ij} \to q_{\rm ij} + s\tilde{\Omega}_{\rm I} \tag{3}$$

with $\tilde{\Omega}_{\rm I} \equiv \frac{\Omega_{\rm I}}{T}$, and averaging over $s = \pm 1$. On the other hand, the contributions of ghosts were found to be indispensable in order to explain confinement at low temperature [38]. How should the imaginary rotation effect be introduced to the ghosts? In the deconfined phase, $\Omega_{\rm I}$ would affect ghosts in a way similarly as physical gluons, but to introduce an effective chemical potential, $il\Omega_{\rm I}$, states with orbital angular momentum (OAM) l are required for the scalar ghosts, while the ones with OAM $l \pm 1$ are required for the transversal gluons [32]. For the origin $r = 0$ [32], it is true that $\Omega_{\rm I}$ does not affect the ghosts as only the states with zero l contribute. However, lattice QCD usually explores the spatial average of PL [29,31], in which case the contributions of the states with $l \neq 0$ could also be important. Take a cylindrical system with radius R for example, we compare the nth eigenenergies $k_{0,n}$ and $k_{1,n}$ that satisfy the boundary condition $J_l(k_{l,n}R) = 0$ in Fig. 1. As can be seen, $k_{1,n}$ is slightly larger than $k_{0,n}$ for a given n. Actually, there are more restrictive unequal relations among the eigenenergies, that is [39],

$$k_{0,n} < k_{1,n} < k_{0,n+1} < k_{1,n+1}, \tag{4}$$

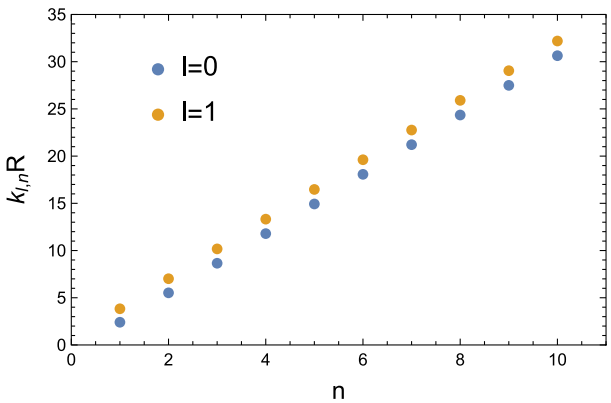

FIG. 1. The nth eigenenergies $k_{l,n}$ that satisfy $J_l(k_{l,n}R) = 0$ for $l = 0$ (blue) and $l = 1$ (yellow).

so $\Omega_{\rm I}$ could induce a remarkable effect to ghosts on average. In light of that, we will intuitively introduce the rotational effect to gluons and ghosts by considering the leading-order nontrivial contributions; that is, the transformations in Eq. (3) would be extended to the thermodynamic potential of confined phase.

For the pure $SU(3)$ gauge theory, the thermodynamic potential is usually presented as a function of PL with the expressions obtained by fitting to lattice simulations [38]. The advantage of such a thermodynamic potential is that the PL can be self-consistently calculated from the gap equation and thus the confinement-deconfinement transition can be well identified from the feature of the order parameter. In the market, there are two most popular parametrizations of the PL potential V, which are

$$\frac{V_1(L,L^*)}{T^4} = -\frac{a(\tilde{T})}{2}|L|^2 - \frac{1.75}{\tilde{T}^3}\ln H(L,L^*),$$
$$a(\tilde{T}) = 3.51 - \frac{2.47}{\tilde{T}} + \frac{15.2}{\tilde{T}^2} \tag{5}$$

given by Fukushima [40] and

$$\frac{V_2(L,L^*)}{T^4} = -\frac{a(\tilde{T})}{2}|L|^2 - \frac{0.75}{6}(L^3+L^{*3}) + \frac{7.5}{4}|L|^4,$$
$$a(\tilde{T}) = 6.75 - \frac{1.95}{\tilde{T}} + \frac{2.625}{\tilde{T}^2} - \frac{7.44}{\tilde{T}^3} \tag{6}$$

given by the Munich group [41]. Here, $\tilde{T} \equiv T/T_0$ is the reduced temperature with $T_0 = 0.27$ GeV, and the Haar measure is defined as [38]

$$H(L,L^*) = 27[1 - 6|L|^2 + 4(L^3+L^{*3}) - 3|L|^4]$$
$$= \prod_{\rm i,j=1,2,3;i>j} |e^{iq_{\rm i}} - e^{iq_{\rm j}}|^2. \tag{7}$$

To effectively introduce rotational effect into the PL potentials, all the terms involved in V_1 and V_2 must be reexpressed as functions of $q_{\rm ij}$. The relevant terms can be rewritten as

$$|L|^2(q_{\rm ij}) = \frac{1}{N_{\rm c}} + \frac{1}{N_{\rm c}^2}\sum_{t=\pm}(e^{tiq_{31}} + e^{tiq_{21}} + e^{tiq_{32}}), \tag{8}$$

$$H(q_{\rm ij}) = \prod_{i,j=1,2,3;i>j}(2 - e^{iq_{\rm ij}} - e^{-iq_{\rm ij}}), \tag{9}$$

$$L^3(q_{\rm ij}) = \frac{1}{N_{\rm c}^3}e^{3iq_1}(1 + e^{iq_{21}} + e^{iq_{31}})^3$$
$$= \frac{1}{N_{\rm c}^3}e^{-i(q_{21}+q_{31})}(1 + e^{iq_{21}} + e^{iq_{31}})^3, \tag{10}$$

$$L^{*3}(q_{\rm ij}) = \frac{1}{N_{\rm c}^3}e^{i(q_{21}+q_{31})}(1 + e^{-iq_{21}} + e^{-iq_{31}})^3; \tag{11}$$

then, the PL potentials become

$$\frac{V_1(q_{\rm ij})}{T^4} = -\frac{a(\tilde{T})}{2}|L|^2(q_{\rm ij}) - \frac{1.75}{\tilde{T}^3}\ln H(q_{\rm ij}), \tag{12}$$

$$\frac{V_2(q_{\rm ij})}{T^4} = -\frac{a(\tilde{T})}{2}|L|^2(q_{\rm ij}) - \frac{0.75}{6}[L^3(q_{\rm ij}) + L^{*3}(q_{\rm ij})]$$
$$+ \frac{7.5}{4}[|L|^2(q_{\rm ij})]^2. \tag{13}$$

So, by applying the variable transformations in Eq. (3), the PL potentials with imaginary rotation effect are, respectively,

$$\bar{V}_1(q_{\rm ij},\Omega_{\rm I}) = \frac{1}{2}\sum_{s=\pm}V_1(q_{\rm ij} + s\Omega_{\rm I}), \tag{14}$$

$$\bar{V}_2(q_{\rm ij},\Omega_{\rm I}) = \frac{1}{2}\sum_{s=\pm}V_2(q_{\rm ij} + s\Omega_{\rm I}). \tag{15}$$

Eventually, recalling that in Ref. [32], the color chemical potentials were alternatively expressed as

$$q_{31} = \phi_1, \quad q_{21} = \frac{\phi_1}{2} + \frac{\sqrt{3}}{2}\phi_2, \quad q_{32} = \frac{\phi_1}{2} - \frac{\sqrt{3}}{2}\phi_2 \tag{16}$$

with $\phi_1 \in [0, 2\pi]$ and $\phi_2 \in [-\frac{\phi_1}{\sqrt{3}}, \frac{\phi_1}{\sqrt{3}}]$, and we can further rewrite the PL potentials as functions of ϕ_1 and ϕ_2, that is,

$$V_1(\phi_1,\phi_2,\Omega_{\rm I}) = \bar{V}_1\left(\phi_1, \frac{\phi_1}{2} + \frac{\sqrt{3}}{2}\phi_2, \frac{\phi_1}{2} - \frac{\sqrt{3}}{2}\phi_2, \Omega_{\rm I}\right), \tag{17}$$

$$V_2(\phi_1,\phi_2,\Omega_{\rm I}) = \bar{V}_2\left(\phi_1, \frac{\phi_1}{2} + \frac{\sqrt{3}}{2}\phi_2, \frac{\phi_1}{2} - \frac{\sqrt{3}}{2}\phi_2, \Omega_{\rm I}\right). \tag{18}$$

One can check that $V(\phi_1,\phi_2,\Omega_{\rm I})$ is real valued as it should be, since there is no sign problem for the QCD action with finite $\Omega_{\rm I}$. Thus, we can search for the global minimum of the thermodynamic potentials with respect to ϕ_1 and ϕ_2 in the constrained region, and then the PL L can be evaluated according to Eq. (1). For the latter purpose, we work out $q_{\rm i}$ $(i = 1, 2, 3)$ first as functions of ϕ_1 and ϕ_2 according to Eq. (16), and we have

$$q_1 = -\frac{\phi_1}{2} - \frac{\phi_2}{2\sqrt{3}}, \quad q_2 = \frac{\phi_2}{\sqrt{3}}, \quad q_3 = \frac{\phi_1}{2} - \frac{\phi_2}{2\sqrt{3}}. \tag{19}$$

Note that L is not necessarily real valued at finite $\Omega_{\rm I}$, so we will eventually present the absolute value of L instead. To determine ϕ_1 and ϕ_2, gap equations can be derived by following $\partial V/\partial\phi_1 = \partial V/\partial\phi_2 = 0$, that is,

$$0 = -\frac{ia(\tilde{T})}{8N_c^2}\sum_{t,s=\pm} t[2e^{tiq_{31}^s} + e^{tiq_{21}^s} + e^{tiq_{32}^s}] + \frac{1.75i}{4\tilde{T}^3}\sum_{s=\pm}\left[\frac{2(e^{iq_{31}^s} - e^{-iq_{31}^s})}{2 - e^{iq_{31}^s} - e^{-iq_{31}^s}} + \frac{e^{iq_{21}^s} - e^{-iq_{21}^s}}{2 - e^{iq_{21}^s} - e^{-iq_{21}^s}} + \frac{e^{iq_{32}^s} - e^{-iq_{32}^s}}{2 - e^{iq_{32}^s} - e^{-iq_{32}^s}}\right], \tag{20}$$

$$0 = -\frac{\sqrt{3}ia(\tilde{T})}{8N_c^2}\sum_{t,s=\pm} t(e^{tiq_{21}^s} - e^{tiq_{32}^s}) + \frac{1.75\sqrt{3}i}{4\tilde{T}^3}\sum_{s=\pm}\left(\frac{e^{iq_{21}^s} - e^{-iq_{21}^s}}{2 - e^{iq_{21}^s} - e^{-iq_{21}^s}} - \frac{e^{iq_{32}^s} - e^{-iq_{32}^s}}{2 - e^{iq_{32}^s} - e^{-iq_{32}^s}}\right) \tag{21}$$

for $V_1(\phi_1, \phi_2, \Omega_{\rm I})$ with $q_{\rm ij}^s = q_{\rm ij} + s\Omega_{\rm I}$ and

$$0 = \sum_{t,s=\pm}\left\{-\frac{ia(\tilde{T})}{8N_c^2}t[2e^{tiq_{31}^s} + e^{tiq_{21}^s} + e^{tiq_{32}^s}] + \frac{0.75i}{8N_c^3}t[e^{-ti(q_{21}^s+q_{31}^s)}(1 + e^{tiq_{21}^s} + e^{tiq_{31}^s})^2(1 - e^{tiq_{31}^s})]\right.$$
$$\left. + \frac{7.5i}{4N_c^2}t\left(e^{tiq_{31}^s} + \frac{1}{2}e^{tiq_{21}^s} + \frac{1}{2}e^{tiq_{32}^s}\right)|L|^2(q_{\rm ij}^s)\right\}, \tag{22}$$

$$0 = \sum_{t,s=\pm}\left\{-\frac{\sqrt{3}ia(\tilde{T})}{8N_c^2}t(e^{tiq_{21}^s} - e^{tiq_{32}^s}) + \frac{0.75\sqrt{3}i}{24N_c^3}t[e^{-ti(q_{21}^s+q_{31}^s)}(1 + e^{tiq_{21}^s} + e^{tiq_{31}^s})^2(1 + e^{tiq_{31}^s} - 2e^{tiq_{21}^s})]\right.$$
$$\left. + \frac{7.5\sqrt{3}i}{8N_c^2}t(e^{tiq_{21}^s} - e^{tiq_{32}^s})|L|^2(q_{\rm ij}^s)\right\} \tag{23}$$

for $V_2(\phi_1, \phi_2, \Omega_{\rm I})$.

Finally, the formalism with real rotation Ω can be obtained from the one with imaginary rotation $\Omega_{\rm I}$ by taking the analytic continuation: $\Omega_{\rm I} \to -i\Omega$. One can easily check that the thermodynamic potential $V(\phi_1, \phi_2, -i\Omega)$ is still real valued, so we can pin down the ground state by minimizing $V(\phi_1, \phi_2, -i\Omega)$ over ϕ_1 and ϕ_2. It is easy to see from the exponentials

$$e^{tiq_{\rm ij}^s} \to e^{t(iq_{\rm ij} + s\Omega)} \tag{24}$$

that real rotation Ω functions as a real chemical potential to gluons and ghosts. Usually, gluons tends to break confinement, while ghosts tends to reinforce it in the language of lattice QCD. So, recalling that the contributions of ghosts are larger than those of gluons at low temperature [38], one might expect that Ω favors confinement when both numbers of gluons and ghosts increase with Ω. As mentioned in Ref. [23], the boundary effect has to be taken into account self-consistently for real rotation in order to satisfy the causality. Here, since there is no summation over transversal eigenenergy in the empirical PL potentials, we simply neglect that.

B. Numerical results

For the Polyakov loop potentials $V_1(\phi_1, \phi_2, \Omega_{\rm I})$ and $V_2(\phi_1, \phi_2, \Omega_{\rm I})$ just developed, the corresponding numerical results are presented in Secs. II B 1 and II B 2, respectively.

1. Polyakov loop potential V_1

In Fig. 2, we demonstrate the PL $|L|$ as a function of temperature T for several imaginary rotations. As can be seen, $\Omega_{\rm I}$ tends to suppress $|L|$ for all T, and the deconfinement transition is of first order—both features are consistent with the predictions of perturbative calculations [38]. Remember that the transition is of strong first order at $\Omega_{\rm I} = 0$ for V_1 [40], so it is not surprising that it remains of first order even when $\Omega_{\rm I}$ is large. In fact, the imaginary rotation effect is quite nontrivial in the Haar

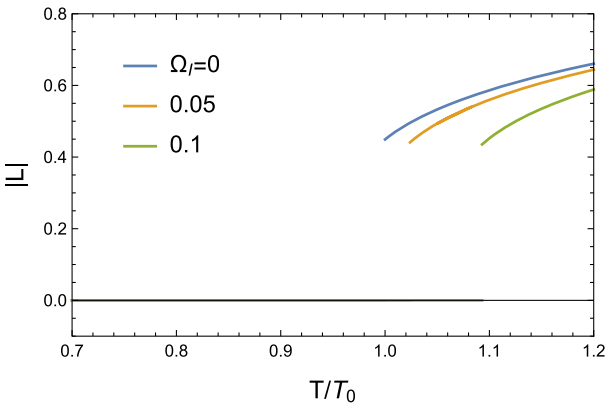

FIG. 2. The absolute value of Polyakov loop, $|L|$, as a function of temperature T for imaginary rotations $\Omega_{\rm I} = 0$, 0.05 and 0.1 GeV.

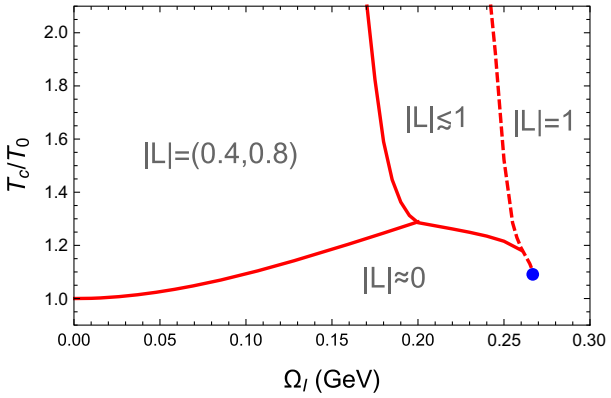

FIG. 3. The temperature-imaginary rotations ($T-\Omega_I$) phase diagram. The solid and dashed lines correspond to first- and second-order transitions, respectively, and the blue bullet is a critical end point.

measure term, and lots of local minima could be developed with respect to ϕ_1 and ϕ_2 at medium T; hence, several branches of transitions can be involved. For a wider range of Ω_I, the relevant transition temperature is illustrated in Fig. 3, where three branches of transitions can be identified: $|L|\approx 0 \to |L|\approx 0.4$, $|L|\approx 0.8 \to |L|\lesssim 1$, and $|L|\lesssim 1 \to |L|=1$. Though the critical temperature increases with Ω_I for the deconfinement transition $|L|\approx 0 \to |L|\approx 0.4$, as shown in Fig. 2, it decreases with Ω_I for the other transitions, and there is even a critical end point.

For the case with real rotation Ω, we demonstrate the PL $|L|$ as a function of temperature T in Fig. 4 and the critical temperature as a function of Ω in Fig. 5. Comparing Fig. 4 with Fig. 2, we find that real rotation tends to break confinement while imaginary rotation tends to reinforce it, as was shown in the perturbative study [32]. Such an effect of real rotation is opposite to the naive analysis in the end of the previous section and implies that the centrifugal splitting effect overcomes the particle number

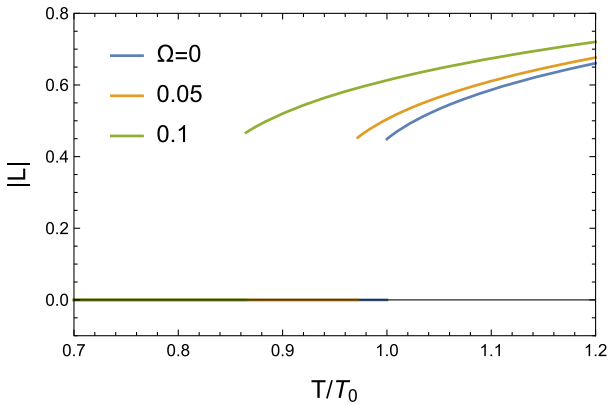

FIG. 4. The absolute value of Polyakov loop, $|L|$, as a function of temperature T for real rotations $\Omega=0$, 0.05, and 0.1 GeV.

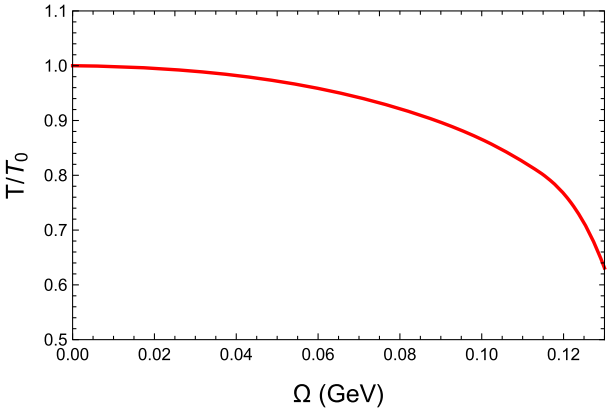

FIG. 5. The temperature-real rotations ($T-\Omega$) phase diagram with the transition of first order.

enhancing effect. Moreover, the mathematical structure of $V_1(\phi_1,\phi_2,-i\Omega)$ as a function of ϕ_1 and ϕ_2 is much simpler than that of $V_1(\phi_1,\phi_2,\Omega_I)$ for given rotations, so only one branch of the first-order phase transition shows up in Fig. 5. Since this branch corresponds to the deconfinement transition $|L|\approx 0 \to |L|\approx 0.4$ in Fig. 2, analytic continuation of the phase diagram from imaginary to real rotations seems to be valid here.

2. Polyakov loop potential V_2

We demonstrate the PL $|L|$ as a function of temperature T for different imaginary rotations in Fig. 6. As can be seen, Ω_I tends to enhance $|L|$ at a relatively small T, consistent with lattice simulations [29,31], but suppresses it at a relatively large T, consistent with perturbative calculations [38]. In fact, the sign change of $a(\tilde{T})$ around $T=T_0$ is responsible for such anomalous features: for T a bit larger than T_0, $a(\tilde{T})>0$, and Ω_I reinforces confinement, as has been shown in Ref. [38]; for $T\lesssim T_0$,

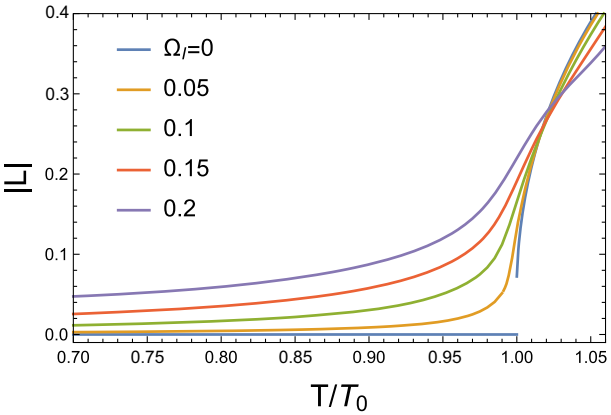

FIG. 6. The absolute value of Polyakov loop, $|L|$, as a function of temperature T for imaginary rotations $\Omega_I=0$, 0.05, 0.1, 0.15, and 0.2 GeV.

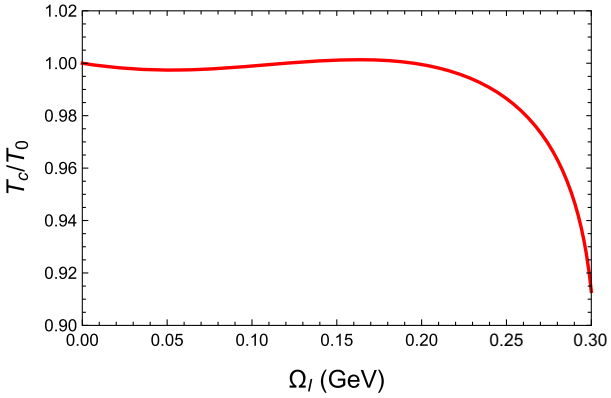

FIG. 7. The temperature-imaginary rotations ($T-\Omega_{\rm I}$) phase diagram with the transition of crossover except for the region with $\Omega_{\rm I}\sim 0$.

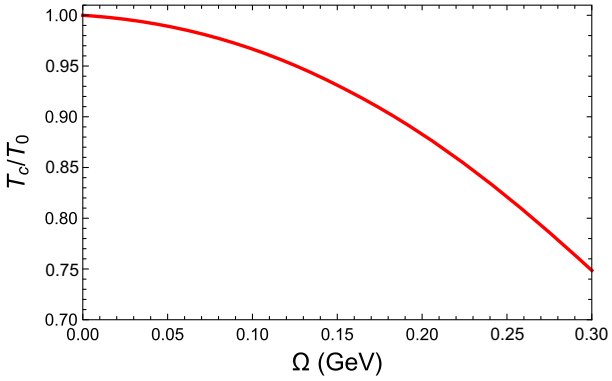

FIG. 9. The temperature-real rotations ($T-\Omega$) phase diagram with the transition of crossover except for the region with $\Omega\sim 0$.

$a(\tilde{T})<0$, and $\Omega_{\rm I}$ breaks confinement. The consistent reverse of the imaginary rotation effect around $T\sim T_0$ is a strong support of the explanation. Since $a(\tilde{T})>0$ for all T in V_1, such a reverse does not show up at all in Fig. 2. Another important observation from Fig. 6 is that the transition is of weak first order at $\Omega_{\rm I}=0$ but becomes crossover for a relatively large $\Omega_{\rm I}$. We can define the pseudocritical temperature $T_{\rm c}$ by the peak of $\partial_T|L|$, and the $T-\Omega_{\rm I}$ phase diagram is illustrated in Fig. 7. Though there is a small oscillation in the phase diagram, the main trend is that $T_{\rm c}$ decreases with $\Omega_{\rm I}$, which is consistent with lattice simulations [29,31]. If the finite boundary effect is self-consistently taken into account, we believe the oscillation would eventually disappear as the transition is smoothed out around $T=T_0$ [29]. In that case, the reverse may also disappear, and the results may become more consistent with lattice simulations.

For the case with real rotation Ω, we demonstrate the PL $|L|$ as a function of temperature T in Fig. 8 and the (pseudo)critical temperature as a function of Ω in Fig. 9.

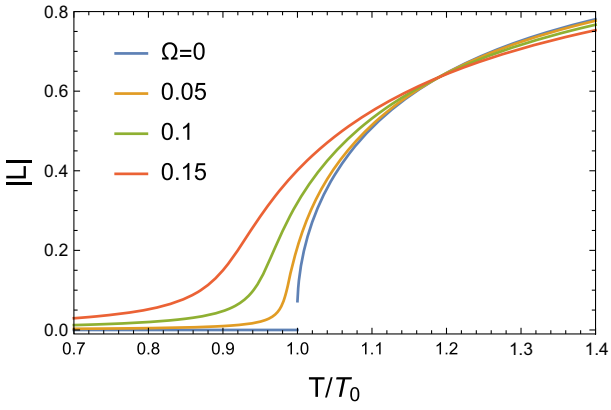

FIG. 8. The absolute value of Polyakov loop, $|L|$, as a function of temperature T for real rotations $\Omega=0$, 0.05, 0.1, and 0.15 GeV.

Contrary to the findings in Sec. II B 1, here the effect of real rotation is the same as that of imaginary rotation on confinement; compare Fig. 8 with Fig. 6 and Fig. 9 with Fig. 7. Still, the opposite features of $|L|$ for $T<1.2T_0$ and $T>1.2T_0$ in Fig. 8 are reflections of sign change of $a(\tilde{T})$ around T_0. And the study in this section provides an example that the analytic continuation of the phase diagram from imaginary to real rotation breaks down. On the other hand, it is interesting that, even though the effect of imaginary rotation diverges from one PL potential to another one, the effects of real rotation are qualitatively the same. The consistency of real rotation effect is meaningful since that is the physical situation we are really interested in.

Why should the effects of imaginary and real rotations be the same whence the second-order contributions of $\Omega_{\rm I}$ and Ω are nonzero for V_2? The point is that the PL potential is not a trivial function of L and L^* anymore when $\Omega_{\rm I}$ or Ω is introduced; rather, it depends on them through the angles ϕ_1 and ϕ_2. Take $\phi_2=0$, which is true for the no-rotation case, for example, the potential V_2 is demonstrated as a function of ϕ_1 for $\Omega_{\rm I}=\Omega=0.05$ GeV and $T/T_0=0.9$, 1 in Fig. 10. Though the minima are both closely located around $\phi_1=\frac{4\pi}{3}$ for $T/T_0=0.9$, the temperature $T=T_0$ tends to shift the minimum to larger ϕ_1 for the imaginary rotation, while it shifts to smaller ϕ_1 for the real rotation. In this sense, the effects of $\Omega_{\rm I}$ and Ω are indeed opposite to each other. However, recalling that $L=0$ for $\phi_1=\frac{4\pi}{3}$, both shifts tend to enhance the absolute value of PL, $|L|=|\frac{1}{3}+\frac{2}{3}\cos\frac{\phi_1}{2}|$—that is exactly what we found in Figs. 6 and 8. Nevertheless, we will see in Sec. III that the two trends would have different consequences on chiral symmetry breaking and restoration when quarks are taken into account.

We summarize the main results about the effects of imaginary (Ω_I) and real (Ω) rotations found from the Polyakov loop potentials V_1 and V_2 in Table. I together with LQCD results.

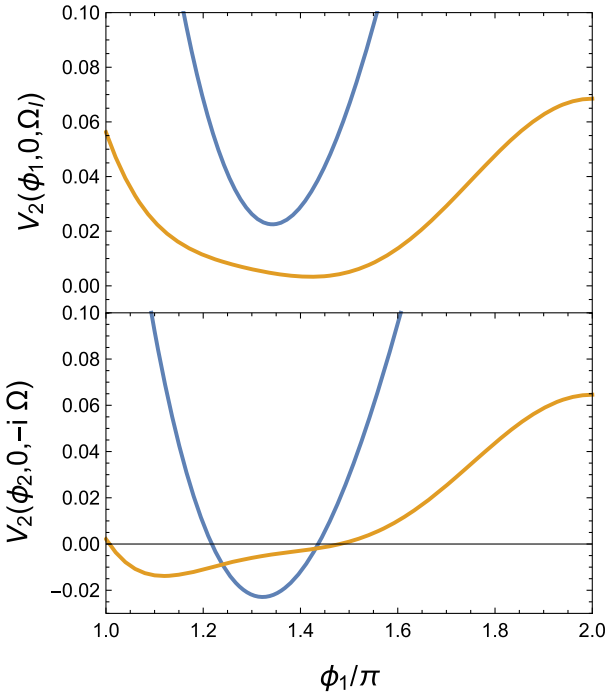

FIG. 10. Assuming $\phi_2 = 0$, the potential V_2 is demonstrated as a function of ϕ_1 for $\Omega_I = 0.05$ GeV (upper panel) and $\Omega = 0.05$ GeV (lower panel) with $T/T_0 = 0.9$ (blue) and 1 (yellow).

III. THREE-FLAVOR POLYAKOV–NAMBU–JONA-LASINIO MODEL

Now, we extend the study to a full QCD matter with gluon degrees of freedom through the modified Polyakov loop potential and three flavors of quarks through NJL model [42,43]. According to the studies in Sec. II, the PL potential V_2 is more consistent with the lattice simulations, so we will adopt it for further explorations in this section. On the other hand, the rotation effects on quark dynamics have been explored for many years in the NJL model [21–23,25–28,44], so we are now armed with the three-flavor Polyakov–Nambu–Jona-Lasinio (PNJL) model where rotation effects are taken into account in both quark and gluon sectors. Note that, unlike the baryon or isospin chemical potential, the rotations can have direct effects on both gluons and quarks, though it functions through effective chemical potentials. However, one should note that there is no interplay between the rotation effects of the two sectors except implicitly through the quark-PL coupling. As a consequence, the model might not reproduce the numerical results of LQCD so well but could definitely help us understand the features qualitatively and physically.

TABLE I. A summary of the effects of imaginary (Ω_I) and real (Ω) rotations, where $\uparrow/\downarrow$ stands for increasing/decreasing and the orders of deconfinement transition are also listed.

	V_1	V_2	LQCD
Ω_I	$T_c\uparrow$ 1st order	$T_c\downarrow$ Crossover	$T_c\downarrow$ Crossover
Ω	$T_c\downarrow$ 1st order	$T_c\downarrow$ Crossover	… …

A. Formalism

By introducing the effect of imaginary rotation, the Lagrangian density of three-flavor PNJL model can be given as [38,42,43]

$$\begin{aligned}\mathcal{L}_{\mathrm{PNJL}} &= \bar{\psi}[i\partial\!\!\!/ - i\gamma^4(ig\mathcal{A}_4 + i\Omega_{\mathrm{I}}(\hat{L}_z + \hat{S}_z)) - m_0]\psi \\ &\quad + G\sum_{a=0}^{8}[(\bar{\psi}\lambda^a\psi)^2 + (\bar{\psi}i\gamma_5\lambda^a\psi)^2] + \mathcal{L}_{\mathrm{tH}} \\ &\quad - V_2(\phi_1,\phi_2,\Omega_{\mathrm{I}}),\end{aligned} \tag{25}$$

where $\psi = (u, d, s)^T$ is the three-flavor quark field with the current mass matrix

$$m_0 \equiv \mathrm{diag}(m_{0\mathrm{u}}, m_{0\mathrm{d}}, m_{0\mathrm{s}}) \tag{26}$$

and $g\mathcal{A}_4$ represents the background $SU(3)$ gauge field. In the imaginary rotation term of quarks, $\hat{L}_z \equiv -i(x_1\partial_2 - x_2\partial_1)$ and $\hat{S}_z \equiv \frac{i}{2}\gamma^1\gamma^2$ are the operators of orbital and spin angular momenta, respectively. In the four-quark interaction terms, the vertices $\lambda^i (i = 1, \ldots, 8)$ are Gell-Mann matrices in flavor space and $\lambda^0 = \sqrt{2/3}1$. For later use, the 't Hooft term $\mathcal{L}_{\mathrm{tH}} \equiv -K\sum_{t=\pm}\mathrm{Det}\bar{\psi}\Gamma^t\psi$ can be reexpressed as [42]

$$\mathcal{L}_{\mathrm{tH}} = -\frac{K}{2}\sum_{t=\pm}\epsilon_{ijk}\epsilon_{imn}(\bar{\psi}^i\Gamma^t\psi^i)(\bar{\psi}^j\Gamma^t\psi^m)(\bar{\psi}^k\Gamma^t\psi^n) \tag{27}$$

with the interaction vertices $\Gamma^{\pm} = \mathbb{1}_4 \pm \gamma_5$ for right- and left-handed channels, respectively. Here, one should note the Einstein summation convention for the flavor indices i, j, k, m, n and the correspondences between 1,2,3, and u, d, s.

For this setup, only $g\mathcal{A}_4$ and the scalar condensates $\sigma_{\mathrm{f}} = \langle\bar{\psi}_{\mathrm{f}}\psi_{\mathrm{f}}\rangle$ $(f = u, d, s)$ are assumed to be nonzero. To facilitate the study, we would like first to reduce $\mathcal{L}_{\mathrm{tH}}$ to an effective form with only four-fermion interactions. By applying the Hartree approximation to contract a pair of quark and antiquark in each term [42], we immediately find

$$\mathcal{L}^4_{\mathrm{tH}} = -K\epsilon_{ijk}\epsilon_{imn}\sigma_i(\bar{\psi}^j\psi^m\bar{\psi}^k\psi^n - \bar{\psi}^j i\gamma^5\psi^m\bar{\psi}^k i\gamma^5\psi^n). \tag{28}$$

Now, the Lagrangian of PNJL model (25) only effectively involves four-quark interactions after substituting $\mathcal{L}_{\mathrm{tH}}$

by $\mathcal{L}^4_{\mathrm{tH}}$. Again, contracting the quark-antiquark pairs in all the four-quark terms, we find the quark bilinear in the form

$$\mathcal{L}^2_{\mathrm{PNJL}} = \bar{\psi}[i\partial\!\!\!/ - i\gamma^4(ig\mathcal{A}_4 + i\Omega_{\mathrm{I}}(\hat{L}_z + \hat{S}_z)) - m]\psi, \tag{29}$$

where the dynamical mass matrix is

$$m = \mathrm{diag}(m_{\mathrm{u}}, m_{\mathrm{d}}, m_{\mathrm{s}}), \tag{30}$$

$$m_{\mathrm{f}} = m_{0\mathrm{f}} - 4G\sigma_{\mathrm{f}} + 2K\sigma_j\sigma_k \tag{31}$$

with $f \neq j \neq k$. The G- and K-dependent terms in Eq. (31) are from the $U_A(1)$ symmetric and anomalous interactions, respectively.

Now, the most important mission is to evaluate the bilinear contribution to the thermodynamic potential in the presence of rotation. To do that, we consider a cylindrical system with radius R and simply set the condensates to be homogeneous across the space. Then, the eigenfunction ψ_{f} $(f = u, d, s)$ can be presented on the basis of eigenstates of $\hat{L}_z$ and transverse helicity $\hat{h}_\perp \equiv \gamma^5\gamma^3\hat{\mathbf{k}}_\perp \cdot \hat{\mathbf{S}}$ as [21]

$$u_{\mathrm{f},\mathrm{k}_\perp,\mathrm{k}_z,\mathrm{l},\mathrm{t}} = \sqrt{\frac{\epsilon_{\mathrm{f}} + m_{\mathrm{f}}}{4\epsilon_{\mathrm{f}}}} e^{ik_z x_3} \begin{pmatrix} \tilde{J}_l \\ t\tilde{J}_{l+1} \\ \frac{k_z - itk_\perp}{\epsilon_{\mathrm{f}} + m_{\mathrm{f}}}\tilde{J}_l \\ \frac{ik_\perp - tk_z}{\epsilon_{\mathrm{f}} + m_{\mathrm{f}}}\tilde{J}_{l+1} \end{pmatrix} \tag{32}$$

$$v_{\mathrm{f},\mathrm{k}_\perp,\mathrm{k}_z,\mathrm{l},\mathrm{t}} = \sqrt{\frac{\epsilon_{\mathrm{f}} + m_{\mathrm{f}}}{4\epsilon_{\mathrm{f}}}} e^{-ik_z x_3} \begin{pmatrix} \frac{k_z - itk_\perp}{\epsilon_{\mathrm{f}} + m_{\mathrm{f}}}\tilde{J}_l \\ \frac{tk_z - ik_\perp}{\epsilon_{\mathrm{f}} + m_{\mathrm{f}}}\tilde{J}_{l+1} \\ \tilde{J}_l \\ -t\tilde{J}_{l+1} \end{pmatrix} \tag{33}$$

with $t = \pm$, the energy $\epsilon_{\mathrm{f}}(k_\perp, k_3) = \sqrt{k_\perp^2 + k_3^2 + m_{\mathrm{f}}^2}$, and $\tilde{J}_l(k_\perp r, \theta) \equiv e^{il\theta}J_l(k_\perp r)$. So, the quark Feynman propagators are

$$G_{\mathrm{f}} = \sum_{t=\pm} u_{\mathrm{f},\mathrm{k}_\perp,\mathrm{k}_z,\mathrm{l},\mathrm{t}}\bar{u}_{\mathrm{f},\mathrm{k}_\perp,\mathrm{k}_z,\mathrm{l},\mathrm{t}} \tag{34}$$

on the variable space $k_\perp, k_z$, and l, and then functional integrations of the quark fields can be carried out to give [21]

$$\Omega_{\mathrm{bl}} = -\sum_{\mathrm{f=u,d,s}}\sum_{l=-\infty}^{\infty}\int\frac{dk_\perp^2}{2\pi}\int\frac{\mathrm{d}k_3}{2\pi}\int_0^R\frac{r\mathrm{d}r}{R^2}[J_l^2(k_\perp r) + J_{l+1}^2(k_\perp r)]\left\{N_{\mathrm{c}}\epsilon_{\mathrm{f}} + T\sum_{\mathrm{j}=1}^{3}\sum_{u=\pm}\ln\left[1 + e^{-\tilde{\epsilon}_{\mathrm{f}} + ui(q_j + (l+\frac{1}{2})\tilde{\Omega}_{\mathrm{I}})}\right]\right\} \tag{35}$$

with $\tilde{\epsilon}_{\mathrm{f}} \equiv \epsilon_{\mathrm{f}}/T$. For $\tilde{\Omega}_{\mathrm{I}} = 0$, recall the normalization property $\sum_{l=-\infty}^{\infty} J_l^2(k_\perp r) = 1$; the thermodynamic potential can be reduced to

$$\Omega_{\mathrm{bl}} = -2\sum_{\mathrm{f=u,d,s}}\int\frac{dk_\perp^2\mathrm{d}k_3}{8\pi^2}\left\{N_{\mathrm{c}}\epsilon_{\mathrm{f}} + T\sum_{\mathrm{j}=1}^{3}\sum_{u=\pm}\ln\left[1 + e^{-\tilde{\epsilon}_{\mathrm{f}} + uiq_j}\right]\right\}. \tag{36}$$

This is exactly the same as the one given in Ref. [38] except that the integration variables are now taken as the transversal momentum $k_\perp$ and longitudinal momentum k_3.

For a finite rotation Ω, the radius should satisfy $R \leq \Omega^{-1}$ for the sake of causality. Then, to average the Bessel functions over transversal space, the boundary condition has to be applied at finite R. In Sec. II A, we have mentioned how the boundary condition can be applied to the bosonic fields; here, for a Dirac field, the boundary condition is a little tricky since we cannot require all components of the wave function to vanish. Instead, no net current across the boundary was adopted as the physical boundary condition [23], and we simply have

$$k_{l,n}R = \begin{cases} \xi_{l,n}, & l \geq 0 \\ \xi_{-l-1,n}, & l < 0 \end{cases}, \tag{37}$$

where $\xi_{l,n}$ is the nth zero of $J_l(z)$. So, by altering $k_\perp$ to $k_{l,n}$ and the integration to summation correspondingly, the bilinear term (35) becomes

$$\Omega_{\mathrm{bl}} = -\sum_{\mathrm{f=u,d,s}}\sum_{l=-\infty}^{\infty}\sum_{\mathrm{n}=1}^{\infty}\frac{2/\pi}{R^2J_{l+1}^2(k_{l,n}R)}\int\frac{\mathrm{d}k_3}{2\pi}\int_0^R\frac{r\mathrm{d}r}{R^2}[J_l^2(k_{l,n}r) + J_{l+1}^2(k_{l,n}r)]\left\{N_{\mathrm{c}}\epsilon_{\mathrm{f}} + T\sum_{\mathrm{j}=1}^{3}\sum_{u=\pm}\ln\left[1 + e^{-\tilde{\epsilon}_{\mathrm{f}} + uiq_j}\right]\right\} \tag{38}$$

with the weight for the summation over n follows that given in Ref. [23]. Recalling the properties $\int_0^R \frac{2rdr}{R^2} J_l^2(k_{l,n}r) = \int_0^R \frac{2rdr}{R^2} J_{l+1}^2(k_{l,n}r) = J_{l+1}^2(k_{l,n}R)$, it follows that

$$\begin{aligned}\Omega_{\rm bl} &= -2\sum_{\rm f=u,d,s}\sum_{l=-\infty}^{\infty}\frac{1}{\pi R^2}\sum_{\rm n=1}^{\infty}\int\frac{{\rm d}k_3}{2\pi}\left\{N_{\rm c}\epsilon_{\rm f}+T\sum_{\rm j=1}^{3}\sum_{u=\pm}\ln\left[1+e^{-\tilde{\epsilon}_{\rm f}+ui(q_j+(l+\frac{1}{2})\tilde{\Omega}_{\rm I})}\right]\right\}\\ &= -2\sum_{\rm f=u,d,s}\sum_{l=0}^{\infty}\frac{1}{\pi R^2}\sum_{\rm n=1}^{\infty}\int\frac{{\rm d}k_3}{2\pi}\left\{2N_{\rm c}\epsilon_{\rm f}+T\sum_{\rm j=1}^{3}\sum_{u,t=\pm}\ln\left[1+e^{-\tilde{\epsilon}_{\rm f}+ui(q_j+t(l+\frac{1}{2})\tilde{\Omega}_{\rm I})}\right]\right\}. \end{aligned} \tag{39}$$

Here, it is interesting to notice that $\frac{1}{\pi R^2}$ plays a role of degeneracy factor for the summation over n and the corresponding eigenenergies satisfy $k_{l,n}^2 \propto R^{-2}$. This is quite similar to the case with a finite magnetic field [45]: the degeneracy factor is $\frac{|qB|}{2\pi}$ for the higher Landau levels $n \geq 1$, and the corresponding Landau energies are $2n|qB|$. However, the effects of finite size and magnetic field are completely different due to the lowest Landau level, with a vanishing energy, in a magnetic field [45].

In the limit $\Omega_{\rm I} \to 0$, we find that the bilinear potential $\Omega_{\rm bl}$ in Eq. (39) is still R dependent, inconsistent with Eq. (36). The reason is that the boundary condition has not been self-consistently taken into account in Eq. (36) and the form only corresponds to the thermodynamic limit $R \to \infty$ where the boundary effect is negligible. In this sense, Eq. (39) must be consistent with Eq. (36) in the limit $R \to \infty$ as the system considered is exactly the same. For $\Omega_{\rm I} = 0$, $T = 0.15$ GeV, and $R = 800$ GeV^{-1}, we have checked numerically that the convergent thermal parts are consistent with each other within an error 0.1%. On the other hand, the vacuum part of the thermodynamic potential is divergent and can be regularized as

$$\Omega_{\rm bl} = -2\sum_{\rm f=u,d,s}\sum_{l=0}^{\infty}\frac{1}{\pi R^2}\sum_{\rm n=1}^{\infty}\int\frac{{\rm d}k_3}{2\pi}\left\{2N_{\rm c}\epsilon_{\rm f}^{\Lambda}+T\sum_{\rm j=1}^{3}\sum_{u,t=\pm}\ln\left[1+e^{-\tilde{\epsilon}_{\rm f}+ui(q_j+t(l+\frac{1}{2})\tilde{\Omega}_{\rm I})}\right]\right\} \tag{40}$$

by adopting the Pauli-Villars scheme, where the regularized vacuum energy is [42]

$$\epsilon_{\rm f}^{\Lambda} = \sum_{j=0}^{3}(-1)^j C_3^j\sqrt{\epsilon_{\rm f}^2+j\Lambda^2}. \tag{41}$$

To facilitate numerical calculations, the integration over k_3 can be carried out for the vacuum part, and the thermal part can be rewritten by utilizing the condition $q_1+q_2+q_3=0$; we have

$$\begin{aligned}\Omega_{\rm bl} = &-\sum_{\rm f=u,d,s}\sum_{l=0}^{\infty}\frac{1}{\pi^2R^2}\sum_{\rm n=1}^{\infty}\left\{N_{\rm c}\sum_{j=0}^{3}(-1)^{j-1}C_3^j(\epsilon_{\rm f0}^2+j\Lambda^2)\ln(\epsilon_{\rm f0}^2+j\Lambda^2)\right.\\ &\left.+2T\sum_{t=\pm}\int_0^{\infty}{\rm d}k_3\left[\ln\left(1+3Le^{-\tilde{\epsilon}_{\rm f}+it(l+\frac{1}{2})\tilde{\Omega}_{\rm I}}+3L^*e^{-2\tilde{\epsilon}_{\rm f}+2it(l+\frac{1}{2})\tilde{\Omega}_{\rm I}}+e^{-3\tilde{\epsilon}_{\rm f}+3it(l+\frac{1}{2})\tilde{\Omega}_{\rm I}}\right)+{\rm c.c.}\right]\right\}\end{aligned} \tag{42}$$

with $\epsilon_{\rm f0} \equiv \epsilon_{\rm f}(k_{l,n},0)$ and $C_2^{-1}=0$.

Eventually, the coupled gap equations of chiral condensates follow directly from the definitions $\sigma_{\rm f} \equiv \langle\bar{q}_{\rm i}q_{\rm i}\rangle = \frac{\partial\Omega_{\rm bl}}{\partial m_{\rm f}}$ as [42]

$$\begin{aligned}\sigma_{\rm f} = &-\frac{2}{\pi^2R^2}\sum_{l=0}^{\infty}\sum_{\rm n=1}^{\infty}\left\{N_{\rm c}m_{\rm f}\sum_{j=0}^{3}(-1)^{j-1}C_3^j\ln(\epsilon_{\rm f0}^2+j\Lambda^2)\right.\\ &\left.-3\sum_{t=\pm}\int_0^{\infty}{\rm d}k_3\frac{m_{\rm f}}{\epsilon_{\rm f}}\left[\frac{Le^{-\tilde{\epsilon}_{\rm f}+it(l+\frac{1}{2})\tilde{\Omega}_{\rm I}}+2L^*e^{-2\tilde{\epsilon}_{\rm f}+2it(l+\frac{1}{2})\tilde{\Omega}_{\rm I}}+e^{-3\tilde{\epsilon}_{\rm f}+3it(l+\frac{1}{2})\tilde{\Omega}_{\rm I}}}{1+3Le^{-\tilde{\epsilon}_{\rm f}+it(l+\frac{1}{2})\tilde{\Omega}_{\rm I}}+3L^*e^{-2\tilde{\epsilon}_{\rm f}+2it(l+\frac{1}{2})\tilde{\Omega}_{\rm I}}+e^{-3\tilde{\epsilon}_{\rm f}+3it(l+\frac{1}{2})\tilde{\Omega}_{\rm I}}}+{\rm c.c.}\right]\right\}.\end{aligned} \tag{43}$$

And the total self-consistent thermodynamic potential of the PNJL model can be found to be [46]

$$\Omega_{\rm PNJL} = 2G\sum_{\rm f=u,d,s}\sigma_{\rm f}^2 - 4K\sigma_{\rm u}\sigma_{\rm d}\sigma_{\rm s} + \Omega_{\rm bl} + V_2(\phi_1,\phi_2,\Omega_{\rm I}) \tag{44}$$

by utilizing the definitions of chiral condensates and their relations to dynamical masses (31). Since $\Omega_{\rm bl}$ also depends on the background gauge fields $q_{\rm i}$ ($i=1,2,3$), the gap equations of ϕ_1 and ϕ_2 follow $\partial\Omega_{\rm PNJL}/\partial\phi_i=0$ ($i=1,2$) as

$$0=-6T\sum_{\rm f=u,d,s}\frac{1}{\pi R^2}\sum_{l=0}^{\infty}\sum_{\rm n=1}^{\infty}\int\frac{{\rm d}k_3}{2\pi}\sum_{t=\pm}\left[\frac{\frac{\partial L}{\partial\phi_i}e^{-\tilde{\epsilon}_{\rm f}+it(l+\frac{1}{2})\tilde{\Omega}_{\rm I}}+\frac{\partial L^*}{\partial\phi_i}e^{-2\tilde{\epsilon}_{\rm f}+2it(l+\frac{1}{2})\tilde{\Omega}_{\rm I}}}{1+3Le^{-\tilde{\epsilon}_{\rm f}+it(l+\frac{1}{2})\tilde{\Omega}_{\rm I}}+3L^*e^{-2\tilde{\epsilon}_{\rm f}+2it(l+\frac{1}{2})\tilde{\Omega}_{\rm I}}+e^{-3\tilde{\epsilon}_{\rm f}+3it(l+\frac{1}{2})\tilde{\Omega}_{\rm I}}}+{\rm c.c.}\right]+\frac{\partial V_2(\phi_1,\phi_2,\Omega_{\rm I})}{\partial\phi_i} \tag{45}$$

with the last term given by the right-hand sides of Eqs. (22) and (23). And according to Eqs. (1) and (19), the derivatives of L can be evaluated as

$$\frac{\partial L}{\partial\phi_1}=\frac{i}{6}(-e^{iq_1}+e^{iq_3}),$$
$$\frac{\partial L}{\partial\phi_2}=\frac{i}{6\sqrt{3}}(-e^{iq_1}+2e^{iq_2}-e^{iq_3}). \tag{46}$$

For the case with real rotation, the thermodynamic potential and gap equations can be directly obtained from Eqs. (42)–(45) by taking the analytic continuation: $\Omega_{\rm I}\to-i\Omega$. At first glance, it seems that the thermal part in Eq. (42) would diverge with increasing l. In fact, it would not if one notices that the eigenenergy $k_{l,n}$ is also l dependent; since $\xi_{l+1,n}>\xi_{l,n}+1$ and $\xi_{0,1}\approx 2.4$, we find $k_{l,n}>(l+1/2)R^{-1}>(l+1/2)\Omega$ after applying the causality condition $\Omega R\le 1$ and the divergence disaster is well avoided. We want to emphasize that by presenting the OAM l in the form of a natural number the imaginary parts cancel out in the thermodynamic potential of quarks even for a real rotation, which means that there is no sign problem at all for the LQCD simulations [38]. To achieve that, it is important that only homogeneous phases are considered and the boundary condition is self-consistently taken into account.

B. Numerical results

Now, we are going to solve the five coupled gap equations for given T and $\Omega_{\rm I}$, that is, three in Eq. (43) and two in Eq. (45). The model parameters can be fixed as

$$m_{0u}=m_{0d}=5.28\ {\rm MeV},\quad m_{0s}=0.124\ {\rm GeV},$$
$$\Lambda=1.13\ {\rm GeV},\quad G=3.51\ {\rm GeV}^{-2},\quad K=-6.50\ {\rm GeV}^{-5} \tag{47}$$

by best fitting to the chiral condensates; pion decay constant; and masses of pion, kaon, and η mesons from the Particle Data Group, that is,

$$\langle\bar{u}u\rangle=\langle\bar{d}d\rangle=(-0.25\ {\rm GeV})^3,\quad f_\pi=93\ {\rm MeV},$$
$$m_\pi=138\ {\rm MeV},\quad m_K=496\ {\rm MeV},\quad m_\eta=548\ {\rm MeV}. \tag{48}$$

Note that we are not able to reproduce the kaon and η masses simultaneously with the Pauli-Villars regularization. So, the model parameters m_{0s} and K are fixed by giving the smallest deviations from the experimental masses, that is, $(\bar{m}_K-m_K)^2+(\bar{m}_\eta-m_\eta)^2$. For the parameters in Eq. (47), it turns out that the best-fitting masses are $\bar{m}_K=0.409$ GeV and $\bar{m}_\eta=0.600$ GeV, respectively. Moreover, the dynamical masses of quarks are $m_{\rm u}^v=m_{\rm d}^v=0.220$ GeV and $m_{\rm s}^v=0.454$ GeV in vacuum, which are all smaller than the ones with hard-cutoff regularization [46].

In the following, we take a small system with radius $R=10\ {\rm GeV}^{-1}$, for example, so that the causality condition allows a rotation velocity as large as 0.1 GeV. For imaginary rotation, the numerical results are illustrated in Fig. 11, which are found to be qualitatively consistent with the LQCD simulations [29,31]. Though the absolute value of the Polyakov loop, $|L|$, increases with temperature

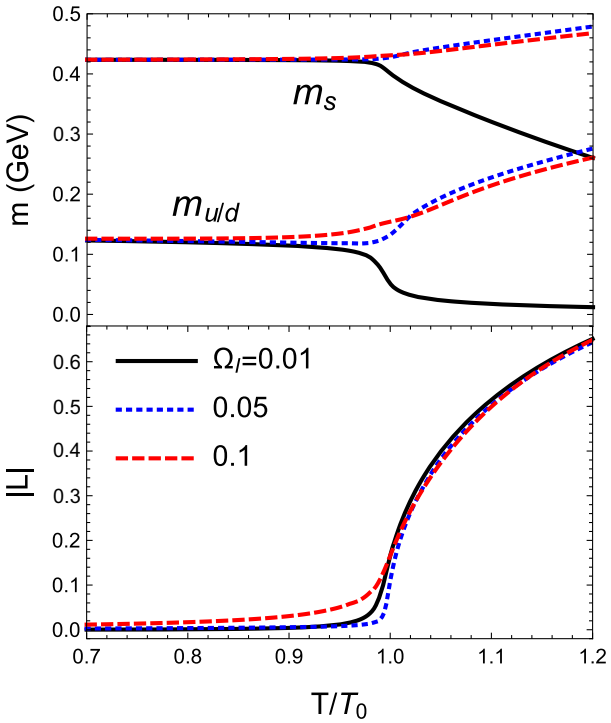

FIG. 11. The masses $m_{\rm f}(f=u,d,s)$ (upper panel) and Polyakov loop $|L|$ (lower panel) as functions of temperature T for imaginary rotations $\Omega_{\rm I}=0.01$ GeV (black solid lines), 0.05 GeV (blue dotted lines), and 0.1 GeV (red dashed lines).

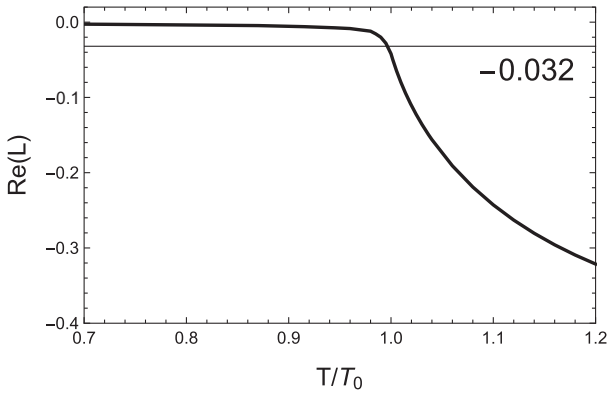

FIG. 12. The real part of the Polyakov loop $\mathrm{Re}(L)$ as a function of temperature with the baseline corresponding to $\mathrm{Re}(L) = -0.032$.

regardless of the value of Ω_I, the features of the dynamical masses or chiral condensates are quite nontrivial; for small Ω_I, $m_\mathrm{f}(f = u, d, s)$ decrease with T, but for large Ω_I, $m_\mathrm{f}(f = u, d, s)$ slightly decrease and then increase with T. The latter feature is unexpected as temperature usually tends to restore chiral symmetry thus reduce dynamical masses [42,43] but is consistent with the LQCD results [31]. The reason of the anomalous behavior is that the real part of the PL, $\mathrm{Re}(L)$, is negative for larger Ω_I and T, contrary to the positive value in general case. As a consequence, the temperature effect can be reversed by the couplings between L/L^* and one/two quark terms in Eq. (42) when

$$\mathrm{Re}[3Le^{-\tilde{\epsilon}_\mathrm{f}+i\frac{1}{2}\tilde{\Omega}_\mathrm{I}} + 3L^*e^{-2\tilde{\epsilon}_\mathrm{f}+2i\frac{1}{2}\tilde{\Omega}_\mathrm{I}} + e^{-3\tilde{\epsilon}_\mathrm{f}+3i\frac{1}{2}\tilde{\Omega}_\mathrm{I}}] < 0. \quad (49)$$

For $\Omega_\mathrm{I} = 0.05$ GeV, we can take $\tilde{\Omega}_\mathrm{I} = 0$ around T_0; then, by adopting the lowest transversal energy $k_{0,1}$ in $\tilde{\epsilon}_\mathrm{f}$, the inequality implies that $\mathrm{Re}(L) < -0.032$. This is roughly consistent with the threshold of increasing masses in the upper panel of Fig. 11; see Fig. 12. Furthermore, according to the results in Fig. 11, the transition becomes crossover when quark degrees of freedom are taken into account, but contrary to the LQCD simulations [31], the pseudocritical temperature increases with Ω_I (though very little). The latter observation indicates that the chiral symmetry breaking effect of Ω_I is stronger than its deconfinement effect in the modified PNJL model. To reproduce the LQCD results better, more realistic PL potential and quark-gluon interplay are needed in the PNJL model.

For the real rotation, the results are illustrated in Fig. 13. The features of $m_\mathrm{f}(f = u, d, s)$ and $|L|$ are all consistent with the initial expectations; that is, $|L|$ increases with both T and Ω due to deconfinement, while $m_\mathrm{f}(f = u, d, s)$ decrease with both T and Ω due to chiral symmetry restoration. The corresponding phase diagram is presented in Fig. 14, in which the pseudocritical temperatures T_c, defined by the peak of the absolute values of the

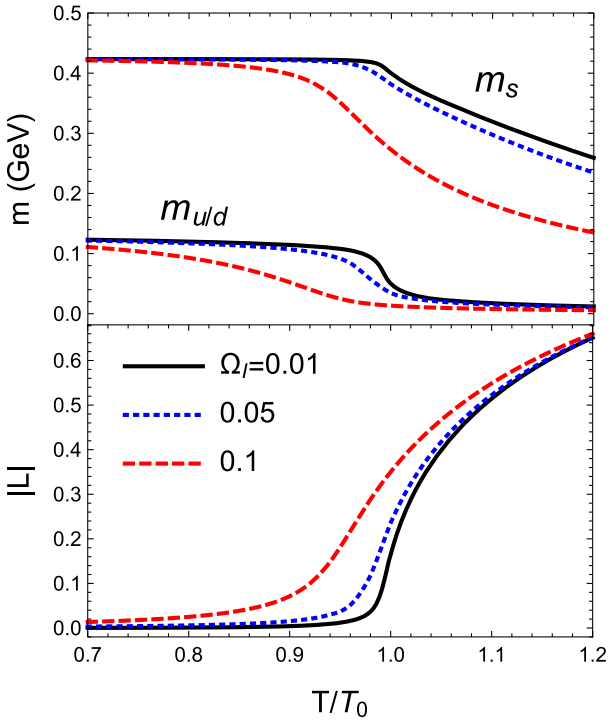

FIG. 13. The masses $m_\mathrm{f}(f = u, d, s)$ (upper panel) and Polyakov loop $|L|$ (lower panel) as functions of temperature T for real rotations $\Omega = 0$ (black solid lines), 0.05 GeV (blue dotted lines), and 0.1 GeV (red dashed lines).

susceptibilities, decrease with Ω as they should [21]. Note that the T_c of the PL $|L|$ is closer to that of s quark dynamical mass m_s. Again, similarly to the pure gauge theory, such effects of real rotation are opposite to those analytically continued from the results of the imaginary rotation [29,31], so the model explorations in Refs. [34,35] are not necessarily unsuccessful. We hope that the LQCD simulations with real rotation can help to settle the issues in the future, as we have shown that there is no sign problem for a special consideration.

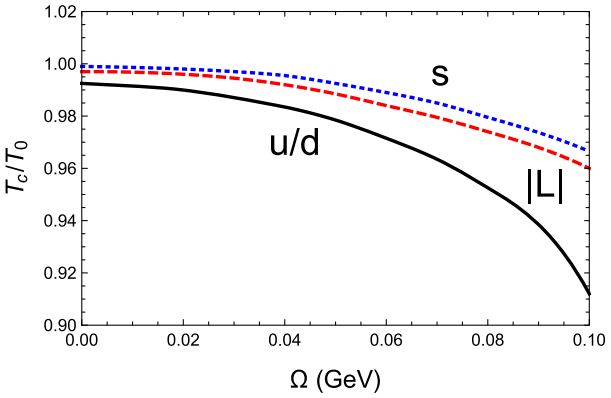

FIG. 14. The pseudocritical temperatures T_c as functions of real rotation Ω for $m_\mathrm{u/d}$, m_s, and $|L|$ in the PNJL model.

IV. SUMMARY

The work is composed of two parts: the pure $SU(3)$ gauge theory and the Polyakov–Nambu–Jona-Lasinio model. Firstly, we try to introduce the rotational effect to the pure $SU(3)$ gauge theory inspired from the perturbative study [32] but without introducing any extra free parameters. Then, the rotational effects on confinement are compared for the two most popular empirical Polyakov loop potentials given by K. Fukushima and Munich's group, respectively. Secondly, the more successful Munich's potential is applied to the chiral effective PNJL model in order to explore the features of chiral symmetry and confinement simultaneously for a QCD matter.

For the first part, the main findings can be summarized as the following: For the PL potential of Fukushima, a smaller imaginary rotation Ω_{I} tends to suppress PL at all temperature and the deconfinement transition keeps of first order. At larger Ω_{I}, two more branches of transitions can be identified: $|L| \approx 0.8 \to |L| \lesssim 1$ of first order and $|L| \lesssim 1 \to |L| = 1$ of second order, both the critical temperatures of which decrease with Ω_{I}. However, for the PL potential of Munich's group, Ω_{I} tends to enhance PL at low temperature T, consistent with lattice simulations [29,31]; but suppress PL at high T, consistent with perturbative calculations [32]. Moreover, we only find one branch of deconfinement transition which alters from first order to crossover with increasing Ω_{I}, expected from lattice simulations [29]. On the other hand, the PL is consistently enhanced by the real rotation Ω at relatively low T in both potentials, and the (pseudo-)critical temperature T_{c} decreases with Ω. Therefore, we at least find an example that the phase diagrams $T - \Omega_{\mathrm{I}}$ and $T - \Omega$ cannot be analytically continued to each other, though Ω_{I} is introduced through analytic continuation of Ω, that is, $\Omega \to i\Omega_{\mathrm{I}}$ [29,31]. The reason is that the PL potential is not a trivial function of L and L^* anymore in the presence of rotations, and any deviation of L/L^* from 0 would enhance $|L|$.

For the second part, we find that the interplays between quarks and gluons render the pseudocritical temperature T_{c} insensitive to Ω_{I} as its effects are opposite from the two sectors while T_{c} decreases with Ω as the effects are the same. For a larger Ω_{I}, we surprisingly find that temperature would further break chiral symmetry as was also presented in the LQCD results [31]. The reason is that $\mathrm{Re}(L)$ becomes more negative with increasing Ω_{I} and the effect of temperature is reversed due to the linear dependences on L and L^* in the logarithmic terms of Ω_{bl}. In the future, we hope the LQCD groups could directly study the real rotation effect by adopting Taylor expansions—that would better help us to understand what is the real situation with rotation.

ACKNOWLEDGMENTS

G. C. thanks Xu-guang Huang and Hao-lei Chen for useful discussions. G. C. is supported by the Natural Science Foundation of Guangdong Province.

[1] F. Becattini, J. Liao, and M. Lisa, Strongly interacting matter under rotation, Lect. Notes Phys. **987**, 1 (2021).
[2] D. T. Son and A. R. Zhitnitsky, Quantum anomalies in dense matter, Phys. Rev. D **70**, 074018 (2004).
[3] M. A. Metlitski and A. R. Zhitnitsky, Anomalous axion interactions and topological currents in dense matter, Phys. Rev. D **72**, 045011 (2005).
[4] D. E. Kharzeev, L. D. McLerran, and H. J. Warringa, The effects of topological charge change in heavy ion collisions: "Event by event P and *CP* violation", Nucl. Phys. **A803**, 227 (2008).
[5] K. Fukushima, D. E. Kharzeev, and H. J. Warringa, The chiral magnetic effect, Phys. Rev. D **78**, 074033 (2008).
[6] K. Landsteiner, E. Megias, L. Melgar, and F. Pena-Benitez, Holographic gravitational anomaly and chiral vortical effect, J. High Energy Phys. 09 (2011) 121.
[7] K. Hattori and Y. Yin, Charge redistribution from anomalous magnetovorticity coupling, Phys. Rev. Lett. **117**, 152002 (2016).
[8] G. Cao, Macroscopic transports in a rotational system with an electromagnetic field, Phys. Rev. D **104**, L031901 (2021).
[9] N. Yamamoto and D. L. Yang, Helical magnetic effect and the chiral anomaly, Phys. Rev. D **103**, 125003 (2021).
[10] Z. T. Liang and X. N. Wang, Globally polarized quark-gluon plasma in non-central A + A collisions, Phys. Rev. Lett. **94**, 102301 (2005).
[11] L. Adamczyk *et al.* (STAR Collaboration), Global Λ hyperon polarization in nuclear collisions: Evidence for the most vortical fluid, Nature (London) **548**, 62 (2017).
[12] F. Becattini and I. Karpenko, Collective longitudinal polarization in relativistic heavy-ion collisions at very high energy, Phys. Rev. Lett. **120**, 012302 (2018).
[13] X. L. Xia, H. Li, Z. B. Tang, and Q. Wang, Probing vorticity structure in heavy-ion collisions by local Λ polarization, Phys. Rev. C **98**, 024905 (2018).
[14] T. Niida (STAR Collaboration), Global and local polarization of Λ hyperons in Au + Au collisions at 200 GeV from STAR, Nucl. Phys. **A982**, 511 (2019).
[15] F. Becattini, G. Cao, and E. Speranza, Polarization transfer in hyperon decays and its effect in relativistic nuclear collisions, Eur. Phys. J. C **79**, 741 (2019).

[16] X. L. Xia, H. Li, X. G. Huang, and H. Z. Huang, Feed-down effect on Λ spin polarization, Phys. Rev. C **100**, 014913 (2019).
[17] W. Florkowski, A. Kumar, A. Mazeliauskas, and R. Ryblewski, Longitudinal spin polarization in a thermal model, Phys. Rev. C **100**, 054907 (2019).
[18] G. Cao and I. Karpenko, Connecting theory to heavy ion experiment, Lect. Notes Phys. **987**, 309 (2021).
[19] F. Becattini, M. Buzzegoli, A. Palermo, G. Inghirami, and I. Karpenko, Local polarization and isothermal local equilibrium in relativistic heavy ion collisions, Phys. Rev. Lett. **127**, 272302 (2021).
[20] B. Fu, S. Y. F. Liu, L. Pang, H. Song, and Y. Yin, Shear-induced spin polarization in heavy-ion collisions, Phys. Rev. Lett. **127**, 142301 (2021).
[21] Y. Jiang and J. Liao, Pairing phase transitions of matter under rotation, Phys. Rev. Lett. **117**, 192302 (2016).
[22] H. L. Chen, K. Fukushima, X. G. Huang, and K. Mameda, Analogy between rotation and density for Dirac fermions in a magnetic field, Phys. Rev. D **93**, 104052 (2016).
[23] S. Ebihara, K. Fukushima, and K. Mameda, Boundary effects and gapped dispersion in rotating fermionic matter, Phys. Lett. B **764**, 94 (2017).
[24] Y. Liu and I. Zahed, Pion condensation by rotation in a magnetic field, Phys. Rev. Lett. **120**, 032001 (2018).
[25] G. Cao and L. He, Rotation induced charged pion condensation in a strong magnetic field: A Nambu–Jona-Lasino model study, Phys. Rev. D **100**, 094015 (2019).
[26] H. L. Chen, X. G. Huang, and K. Mameda, Do charged pions condense in a magnetic field with rotation?, arXiv:1910.02700.
[27] H. Zhang, D. Hou, and J. Liao, Mesonic condensation in isospin matter under rotation, Chin. Phys. C **44**, 111001 (2020).
[28] G. Cao, Charged rho superconductor in the presence of magnetic field and rotation, Eur. Phys. J. C **81**, 148 (2021).
[29] V. V. Braguta, A. Y. Kotov, D. D. Kuznedelev, and A. A. Roenko, Influence of relativistic rotation on the confinement-deconfinement transition in gluodynamics, Phys. Rev. D **103**, 094515 (2021).
[30] M. N. Chernodub, V. A. Goy, and A. V. Molochkov, Inhomogeneity of a rotating gluon plasma and the Tolman-Ehrenfest law in imaginary time: Lattice results for fast imaginary rotation, Phys. Rev. D **107**, 114502 (2023).
[31] J. C. Yang and X. G. Huang, QCD on rotating lattice with staggered fermions, arXiv:2307.05755.
[32] S. Chen, K. Fukushima, and Y. Shimada, Perturbative confinement in thermal Yang-Mills theories induced by imaginary angular velocity, Phys. Rev. Lett. **129**, 242002 (2022).
[33] X. Chen, L. Zhang, D. Li, D. Hou, and M. Huang, Gluodynamics and deconfinement phase transition under rotation from holography, J. High Energy Phys. 07 (2021) 132.
[34] Y. Chen, D. Li, and M. Huang, Inhomogeneous chiral condensation under rotation in the holographic QCD, Phys. Rev. D **106**, 106002 (2022).
[35] H. L. Chen, Z. B. Zhu, and X. G. Huang, Quark-meson model under rotation: A functional renormalization group study, Phys. Rev. D **108**, 054006 (2023).
[36] Y. Jiang, Chiral vortical catalysis, Eur. Phys. J. C **82**, 949 (2022).
[37] K. Mameda and K. Takizawa, Deconfinement transition in the revolving bag model, Phys. Lett. B **847**, 138317 (2023).
[38] K. Fukushima and V. Skokov, Polyakov loop modeling for hot QCD, Prog. Part. Nucl. Phys. **96**, 154 (2017).
[39] M. Abramowitz and I. A. Stegun, *The Handbook of Mathematical Functions with Formulas, Graphs, and Mathematical Tables* (Dover Publications, Washington, D.C., 1964).
[40] K. Fukushima, Chiral effective model with the Polyakov loop, Phys. Lett. B **591**, 277 (2004).
[41] C. Ratti, M. A. Thaler, and W. Weise, Phases of QCD: Lattice thermodynamics and a field theoretical model, Phys. Rev. D **73**, 014019 (2006).
[42] S. P. Klevansky, The Nambu-Jona-Lasinio model of quantum chromodynamics, Rev. Mod. Phys. **64**, 649 (1992).
[43] T. Hatsuda and T. Kunihiro, QCD phenomenology based on a chiral effective Lagrangian, Phys. Rep. **247**, 221 (1994).
[44] L. Wang, Y. Jiang, L. He, and P. Zhuang, Local suppression and enhancement of the pairing condensate under rotation, Phys. Rev. C **100**, 034902 (2019).
[45] G. Cao, Recent progresses on QCD phases in a strong magnetic field: Views from Nambu–Jona-Lasinio model, Eur. Phys. J. A **57**, 264 (2021).
[46] G. Cao, L. He, and P. Zhang, Reentrant pion superfluidity and cosmic trajectories within a PNJL model, Phys. Rev. D **104**, 054007 (2021).